Long-term induced seismicity on the Mosha fault by Damavand Volcano, N-Iran, Implications on the seismic hazard of Tehran metropolis

Seyyedmaalek Momeni[1,2*], Raul Madariaga[3]

1. EPFL Geo-Energy Lab – Gaznat Chair on Geo-Energy, Lausanne, Switzerland.
2. International Centre for Theoretical Physics (ICTP), Trieste, Italy.
3. Labratoire de Geologie, Ecole Normale Superieure, 75231 Paris Cedex 05, France.
***** E-mail: maalek.momeni@gmail.com

Seismic history of the Mosha fault, the most important active fault of Eastern Tehran metropolis, and its relation to the activity of Damavand Volcano, the highest mountain of the Middle-East, is investigated. Historical earthquakes cover the three segments of the Mosha fault by three 6.5<M<7.7 events. Instrumental earthquake catalogs show that the seismicity of the central segment of Mosha fault, close to the Damavand Volcano, is quite high compared to its Western and eastern segments. On May 7th, 2020, an Mw5.1 earthquake struck in the 40 km East of the Tehran, on the central segment of Mosha fault, 10 Km South of Damavand Volcano crest. Its moment tensor obtained by inverting the local broadband displacement waveforms, showing a strike-slip mechanism with N-S and WNW-ESE planes and a centroid depth in 12 km. Its extended rupture imaged on a single elliptical slip patch that nucleates at a depth of 14 km and its slip grows mostly toward up-dip and to the WNW with an average speed of ~2.5 km/s and lasts for ~2.8 s, releasing a total scalar seismic moment of ~4.8E+16 Nm. It exhibits a left-lateral strike-slip mechanism (rake=14°) as expected for the Mosha fault. Early aftershocks (first 45 days), including an M4.1 event, mostly distributed to the up-dip of the slip model showing a strong directivity effect of the mainshock.

We observe a relative seismic silence for the ruptured part of Mosha during 2020 sequence compared to its East and West parts, in the last 14 years, suggesting its partial locking. The occurrence of several instrumental earthquakes on the central segment of Mosha fault in 10 km South of the Damavand Volcano (1930, 1955, and 1983), its recent high microseismic activity, and the 2020 seismic sequence on it, suggest the effect of Volcano on the seismicity of this part of Mosha fault. This idea supported by the existence of a Sill-like young magma chamber of Damavand on the SSW of its crater toward the Mosha fault. The existing heat raises the pore-pressure on the fault, which decreases the effective normal stress and ease the rupture nucleation-expansion. Several hot springs observed in the same area on the Mosha fault that confirms the existence of the magma chamber. The mentioned mechanism may propose that some parts of the central segment of Mosha fault cannot accumulate considerable tectonic strain, while its seismicity rate would be high. In terms of dynamic rupture simulation, Damavand volcano can work as a fuse and nucleate earthquakes on the Mosha fault, for which if the rupture grows toward the West, it will cause a strong directivity effect for that earthquake toward Tehran megacity.

Vicinity of the Mosha fault to Tehran city with >15 million population, its straight length of >150 km, and reported historical earthquakes together with recent seismic activity on it highlight the importance of detail study of this fault system in terms of assessment of seismic hazard of the Tehran city.

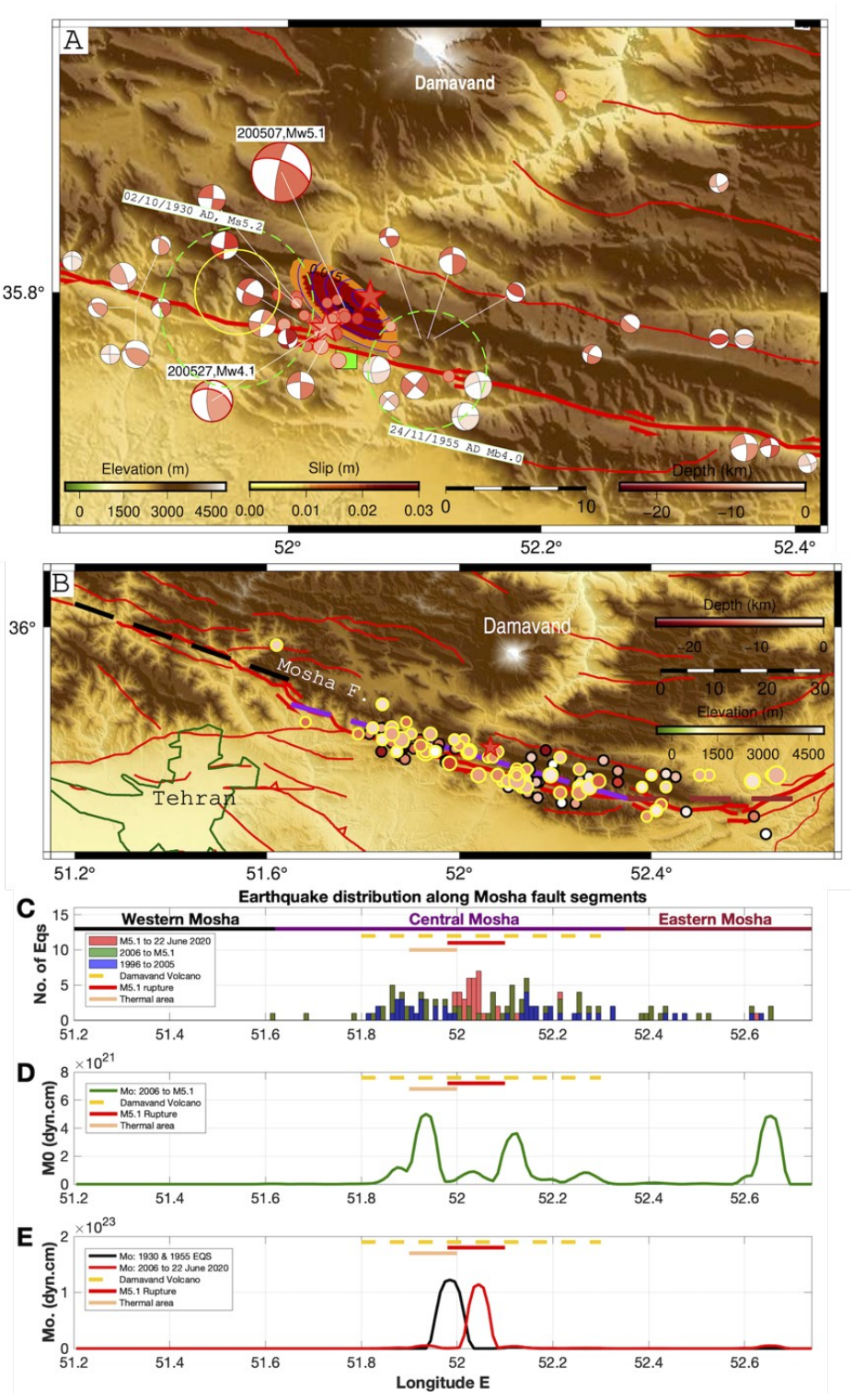

Figure 1. **A:** Correlation between the 7 May 2020 M5.1 mainshock rupture (colored ellipse) and M>2.5 aftershocks of the first 45 days (Red circles). Stars are mainshock and largest aftershock hypocenters relocated in this study. The mainshock focal mechanism is obtained in this study. The M4.1 27/05/2020 aftershock focal mechanism is from IRSC. Inner colors represent their depths. Faults are in red lines. Blue curved lines represent rupture direction. The green square is

the location of Mosha town. The light-green dashed ellipses show the damaged areas of the Ms5.2 1930 and Mb4.0 1955 earthquakes (after Berberian et al., 1993). Other focal mechanisms are from microearthquakes on the Mosha fault obtained by Tatar et al. (2012) from June to October 2006. The yellow circle is the observed thermal area on the Mosha fault (after Eskandari et al., 2018). **B**: Seismicity in the distance of 5 km from the Mosha fault from 1996 until the M5.1 mainshock. Black and Yellow circles are the earthquakes from 1996 to the end of 2005, and 2006 until before the M5.1, respectively. Black, Purple, and brown dashed lines are Western, Central, and Eastern segments of the Mosha fault, respectively. **C**: Histogram showing the distribution of earthquakes along the Mosha fault. **D**: Distribution of scalar seismic moments along the Mosha fault from 2006 until before the 2020 M5.1 mainshock. **E**: Distribution of scalar seismic moments along Mosha fault from 2006 until 22 June 2020, including the M5.1 mainshock and 29 M>=2.5 early aftershocks.

References

Abbassi, M.R. & Farbod, Y., 2009. Faulting and folding in quaternary deposit of Tehran's piedmont (Iran). Journal of Asian Earth Sciences, **34**, 522–531.

Ambraseys, N.N. & Melville, C.P., 1982. A History of Persian Earthquakes, Cambridge Univ. Press.

Berberian, M. & Yeats, R.S., 1999. Patterns of historical earthquake rupture in the Iranian Plateau. Bulletin of the Seismological Society of America **89**, 120–139.

Berberian, M. & Yeats, R.S., 2001. Contribution of archaeological data to studies of earthquake history in the Iranian Plateau. Journal of Structural Geology **23**, 563–584.

Berberian, M., 1997. Seismic sources of the Transcaucasian historical earthquakes, in Historical and Prehistorical Earthquakes in the Caucasus, pp. 233–311, eds., Giardini, S. & Balassanian, S., Kluwer Academic Publishing, Dordrecht, Netherlands.

Bouchon, M., 2003. A Review of the Discrete Wavenumber Method ,2003, Pure appl. geophys. 160, 445–465 0033 – 4553/03/040445–21.

Cotton, F. & Coutant, O., 1997. Dynamic stress variations due to shear faults in a plane-layered medium, Geophys. J. Int., **128**, 676–688.

Davidson, J., Hassanzadeh, J., Berzins, R., Stockli, D. F., Bashukooh, B., Turrin, B. & Pandamouz, A., 2004. The geology of Damavand volcano, Alborz Mountains, northern Iran. *GSA Bulletin*; **116** (1-2), 16–29. doi: https://doi.org/10.1130/B25344.1

Djamour, Y., Vernant, P., Bayer, R., Nankali, H.R., Ritz, J.F., Hinderer, J., Hatam, Y., Luck, B., Le Moigne, N., Sedighi, M. & Khorami, F., 2010. GPS and gravity constraints on continental deformation in the Alborz mountain range, Iran, Geophys. J. Int, **181**, 1287-1301.

Engdahl, E.R., Van der Hilst, R. & Buland, R., 1998. Global teleseismic earthquake relocation with improved travel times and procedures for depth determination. Bulletin of the Seismological Society of America **88**, 722–743.

Eskandari, A., Amini, S., De Rosa, R. & Donato, P., 2018. Nature of the magma storage system beneath the Damavand volcano (N. Iran): An integrated study. S0024 4937(17)30423-1. doi: 10.1016/j.lithos.2017.12.002

Goebel, T.H.W., Weingarten, M., Chen, X., Haffener, J., Brodesky, E.E., 2017. The 2016 Mw5.1 Fairview, Oklahoma earthquakes: Evidence for long-range poroelastic triggering at >40 km from fluid disposal wells, Earth and Planetary Science Letters, 472, 50-61.

Lienert, B.R. & Havskov, J., 1995. A computer program for locating earthquakes both locally and globally, *Seismol. Res. Lett*., **66**, 26–36.

Mostafanejad A, Shomali ZH & Mottaghi AA., 2011. 3-D velocity structure of Damavand volcano, Iran, from local earthquake tomography. J Asian Earth Sci **42**, 1091–1096. doi: 10.1016/j. jseaes.2011.03.011

Momeni, S.M., Aoudia, A., Tatar, M., Twardzik, C. & Madariaga, R., 2019. Kinematics of the 2012 Ahar–Varzaghan complex earthquake doublet (M_w6.5 and M_w6.3), *Geophysical Journal International*, **217**, 2097–2124, https://doi.org/10.1093/gji/ggz100

Nazari, H., Ritz, J.-F., Shafei, A., Ghassemi, A., Salamati, R., Michelot, J.-L. & Massault, M., 2009. Morphological and paleoseismological analyses of the Taleghan fault, Alborz, Iran. Geophysical Journal International. doi:10.1111/j1365-246x.2009.04173. x.

Saar, M.O., Manga, M., 2003. Seismicity induced by seasonal groundwater recharge at Mt. Hood, Oregon, Earth and Planetary Science Letters, 214, 605-618.

Shomali, Z. H. & Shirzad, T., 2014. Crustal structure of Damavand volcano, Iran, from ambient noise and earth- quake tomography. Journal of Seismology **19**, 191-200.

Stocklin, J., 1974. Possible ancient continental margin in Iran. In: Burke, C., Drake, C. (Eds.), Geology of Continental Margins. Springer-Verlag, New York, 873–877.

Ruiz, S., & Madariaga, R., 2013. Kinematic and dynamic inversion of the 2008 northern Iwate earthquake, Bull. Seismol. Soc. Am., **103**(2A), 694–708, doi: 10.1785/0120120056.

Ruiz, S., Ammirati, J.B., Leyton, F., Cabrera, L., Potin, B. & Madariaga, R.,2019. The January 2019 (Mw 6.7) Coquimbo Earthquake: Insights from a Seismic Sequence within the Nazca Plate. *Seismological Research Letters*; **90** (5): 1836–1843.

Sambridge, M., 1999a. Geophysical inversion with a neighborhood algorithm—I. Searching a parameter space, Geophysical. J. Int., **138**, 479–494.

Sambridge, M., 1999b. Geophysical inversion with a neighborhood algorithm—II. Appraising the ensemble, Geophysical. J. Int., **138**, 727–746.

Scuderi, M.M., Collettini, C., Marone, C., 2017. Frictional stability and earthquake triggering during fluid pressure stimulation of an experimental fault, Earth and Planetary Science Letters, **477**, 84-96.

Sokos, E. & Zahradník, J., 2008. ISOLA a Fortran code and a Matlab GUI to perform multiple-point source inversion of seismic data, *Computers and Geosciences*, **34**, 967-977.

Tatar, M., Hatzfeld, D., Abbassi, A. & YaminiFard, F., 2012. Microseismicity and seismotectonics around the Mosha fault (Central Alborz, Iran), Tectonophysics, **544–545**, 50-59.

Vernant, P., Nilforoushan, F., Hatzfeld, D., Abassi, M.R., Vigny, C., Masson, F., Nankali, H., Martinod, J., Ashtiani, M., Bayer, R., Tavakoli, F. & Chéry, J., 2004a. Present-day crustal deformation and plate kinematics in the Middle East constrained by GPS measurements in Iran and northern Oman. Geophysical Journal International **157**, 381–398.

Vernant, P., Nilforoushan, F., Chéry, J., Bayer, R., Djamour, Y., Masson, F., Nankali, H.,

Ritz, J.-F., Sedighi, M. & Tavakoli, F., 2004b. Deciphering oblique shortening of central Alborz in Iran using geodetic data. Earth and Planetary Science Letters, **223**, 177–185.

Yagi, Y., Okuwaki, R., Enescu, B. *et al.* Rupture process of the 2016 Kumamoto earthquake in relation to the thermal structure around Aso volcano. *Earth Planet Sp,* **68,** 118 (2016). https://doi.org/10.1186/s40623-016-0492-3.

Yazdanparast, M. and Vosooghi, B., 2014. A research on Damavand magma source model using GPS data, Geomatics, Natural Hazards and Risk, 5:1, 26-40, DOI: 10.1080/19475705.2013.772543.

Zhu, W., Allison, K.L., Dunham, E.M., Yang, Y., 2020. Fault Valving and Pore Pressure Evolution in Simulations of Earthquake Sequences and Aseismic Slip, Computational Physics. https://arxiv.org/abs/2001.03852.

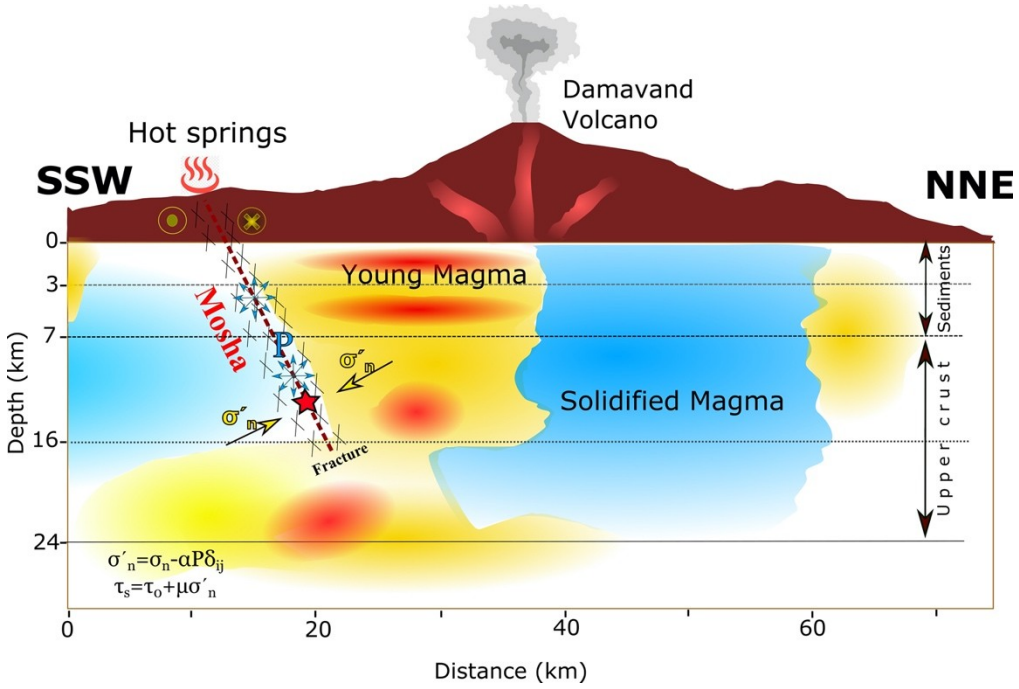

Graphical Abstract. Schematic plot illustrates the relation between Mosha fault and Damavand Volcano. Red and Blue represent the hot and cooled magma of Damavand, respectively (after Mostafanejad et al., 2011, Shomali & Shirzad, 2014, Yazdanparast & Vosooghi, 2014, Vajedian et al., 2015, Eskandari et al., 2018). The red star is the 7th May 2020 M5.1 mainshock hypocenter. Red dashed line is the Mosha fault. Horizontal dashed lines are crustal velocity layers from Tatar et al. (2012).